Project Title:	Generalizable Mechanistic Understanding of Module-Level Light-Moisture and Thermal-Induced Instabilities in CIGS Photovoltaics
Project Period:	10/1/15-03/31/20
Submission Date:	03/25/2021
Recipient:	Board of Trustees of the University of Illinois pre 1/1/17
	Board of Trustees, Colorado School of Mines post 1/1/17
Address:	1500 Illinois St., Golden CO 80401-1887
Award Number:	DE-EE0007141
Project Team:	University of Illinois / Colorado School of Mines
	The Ohio State University
	Old Dominion University
Principal Investigator:	Angus Rockett Phone: 303-384-2244 Email: arockett@mines.edu
Business Contact:	Ralph L. Brown, Phone 303-273-3538, rabrown@mines.edu

Acknowledgement: "This material is based upon work supported by the Department of Energy, Office of Energy Efficiency and Renewable Energy, Solar Energy Technologies Office, , under Award Number DE-EE0007141.

Generalizable Mechanistic Understanding of Module-Level Light-Moisture and Thermal-Induced Instabilities in CIGS Photovoltaics

EERE Project DE-EE0007141

Principal Investigators:

Angus Rockett, Colorado School of Mines;

Aaron Arehart, The Ohio State University; and

Sylvain Marsillac, Old Dominion University

TABLE OF CONTENTS

Objectives and Budget Period Summary

The objectives of this project are to identify the root causes of light, heat and humdity induced instabilities in the operation and accelerated testing of commercial $Cu(In,Ga)Se_2$ [CIGS] photovoltaic modules produced by major module manufacturers (e.g.: Solibro and MiaSolé), correlate them with module degradation/failure modes, and produce accurate service lifetime prediction models.

Budget Period 1: During BP1, we established that we can observe changes due to instabilities, determined the best methods to use, and showed how the changes in the device relate to structure and properties. This was completed as part of the contract at the University of Illinois.

During the first budget period staff was hired and trained in basic analysis methods, and samples were obtained from commercial partners. Preliminary analyses of the samples were conducted. We obtained samples from Solibro and MiaSolé and visited two other partners to establish and maintain relations, to discuss the objectives of the project, and plan for obtaining samples from NuvoSun and Stion. Because of changes in the relationship of NuvoSun to Dow that interaction was limited and eventually terminated, but Rockett visited with the NuvoSun and Stion following those initial meetings and kept in touch with the staff at those two organizations while they were in business. Some samples from these companies continued to be available through NREL with the manufacturer's permission and were tested at NREL under existing agreements. Because of very strong consistent willingness of MiaSolé and its staff to work with us we focused on working with them. They provided samples, discussed results, and worked with us to improve our analyses of their materials. We continued to work with Solibro. We analyzed CIGS devices showing varied levels of instability using large area imaging methods and test facilities at NREL, with capacitance methods at Ohio State, and at ILLINOIS and the Colorado School of Mines. With some analytical techniques, we also studied CdTe devices for comparison and have found dramatic differences between the CIGS and CdTe behaviors. We fabricated materials at Old Dominion University and tested their sensitivity to humidity in the various layers in the CIGS devices. The major sensitivity to humidity was found for the CIGS layer prior to CdS deposition and in the Mo layer before the CIGS deposition.

Budget Period 2: We followed up on the basic approaches and understandings developed previously and established the mechanisms of instability and how process or material changes affect them. We tested preliminary models for light-induced instability (LII) and heat and humidity-induced instability (HHII) degradation and worked with commercial suppliers to transfer the knowledge gained to their staff.

During the second budget period we developed a deeper understanding of the mechanisms of instability. We created and tested preliminary models for metastability and found these to be consistent with our experimental results. We established the fundamental mechanisms for metastability related to two defect states, one at ~980 meV above the valence band and one ~560 meV above the valence band. These are discussed in detail later in this report. We showed that the behavior is general in all samples analyzed rather than being associated with a specific localized area of the material. Commercial materials were found to be very uniform and homogeneous. The large-area measurements made on full modules confirmed this. The results imply that metastability is associated with nanoscale properties of the material rather than localized macro or mesoscale defects. Studies of how process parameters affect these defects were completed in the third phase of the project.

We showed that there is no obvious macroscale or mesoscale defect in CIGS associated with metastability either under light or humidity. We studied full scale modules under illumination by electroluminescence. While we detected differences from one module or device to another in large areas, we did not find any local area or defect controlling those differences. We showed that degradation can occur if local shadowing occurs and demonstrated the mechanisms for that degradation. Specifically, we observed that shadowed areas produce high reverse voltages on monolithic interconnects. This leads to formation of "worm tracks", serpentine defects around the edges of the interconnects. Our observations differed somewhat from those of other groups in the way that the defects formed and propagated. Details are provided below on these observations.

Budget Period 3: During the final budget period we refined our models of instabilities and degradation processes in the various layers of CIGS cells/modules based on the SCAPS computer code to model experimental results. We established several key correlations with experimental variables and verified them by comparison to numerical models.

No cost Extension:

Because of a significant delay in shifting the project from the University of Illinois to the Colorado School of Mines, combined with the start date that missed our ability to bring on new graduate students for most of the first year the project expenditures were significantly delayed. Therefore the project, originally intended to end in August 2018 was extended to December 2019. While this had some impact on the initial productivity the end result of the project was that we accomplished everything that was intended and demonstrated a variety of important results.

Project timeline: Inception July, 2015 Little effort in Q1 & Q2 due to establishing contracts and hiring staff

Novation to CSM: Summer 2016

End of the project: December 2019

Training:

A variety of students and post-docs were engaged on this project. At the University of Illinois prior to transfer of the project to the Colorado School of Mines three students were engaged in the project, Shayla Bhuiya, Thomas Erickson, and Mohit Tuteja. Ms. Bhuiya transferred out of the group within the first nine months. Mr. Erickson completed a Masters Degree during the first year. Dr. Tuteja completed a Ph.D. during the second year of the project. His research consisted of scanning microwave impedance microscopy and other measurements with the relevant results described elsewhere in this document. At the Ohio State University the primary graduate student on the project was Pran Paul with assistance by Julia Deitz. Dr. Paul completed a Ph.D. degree based on research funded primarily by this project and now works at Intel. Dr. Deitz was primarily working on a different project but helped with this project part time. She graduated and is now working at NREL. Other minor contributions were made to the project by Kevin Galiano and Christine Jackson, both of whom have graduated. At the Old Dominion University Shankar Karki and Grace Rajan supported the project based on funds provided by Old Dominion as well as by the project. Both graduated with Dr. Rajan completing a Ph.D degree in 2018 and Dr. Karki finishing a Ph.D in 2019 based on their research under this project. Finally, after transfer of the project to the School of Mines the project was carried on by Mr. Jake Wands supported by Ms. Elizabeth Palmiotti, and Dr. Sina Soltanmohammad. Mr. Wands and Ms. Palmiotti continue their Ph.D research in related areas and Dr. Soltanmohammad completed his post-doc and has moved on to a job in the microelectronics area in California. Finally, Mason Brevig was an undergraduate research assistant who worked with Dr. Soltanmohammad to conduct the Raman measurements.

Summary of the Major Conclusions

The primary conclusions of this project are as follows:

1. Demonstration of a trap state near the conduction band edge (E_V+0.98 eV) in CIGS and demonstration and modeling showed this state is likely the V_{Cu}-V_{Se} divacancy that compensates doping and can lead to light- and heat-induced J_{SC} instability. Furthermore, we showed that this defect is reduced by annealing or post-deposition alkali (K, Na, and Rb) treatments.
2. Demonstration of a trap state near midgap in CIGS whose trap energy is constant relative to the conduction band (E_C-0.72 eV). The energy relative to the conduction band varies with the (A)CIGS bandgap. This state was shown to likely be a recombination center reducing open circuit voltage, V_{oc}, causing light-induced V_{OC} instability, and whose concentration was unaffected by alkali halide treatments and other growth conditions. Only annealing led to moderate reduction.
3. Comparative study of films and devices produced at MiaSole HiTech, Solibro, and others and demonstration that these materials are mostly identical in their behaviors with only quantitative differences in the electrically active defect concentrations.
4. Demonstration that the near mid-gap E_C-0.72 and near valence band E_V+0.98 eV traps could solely explain the light- and heat-induced J_{SC} and V_{OC} instabilities.
5. Study of the effect of moisture on the device when exposure occurs at various stages of the deposition process. Even extended soaking in water had little effect on the device except when the Mo back contact was exposed to the water.
6. Demonstration of metastable changes in the Raman spectrum of CIGS on light soaking, hypothesized to indicate metastable changes in the divacancy defect structure.
7. Study of shadowing on full modules and demonstration that macroscopic defects are not primarily responsible for the metastable behaviors observed in CIGS devices. Demonstration of the mechanism of degradation based on formation of “worm tracks” from the monolithic interconnects as part of the breakdown failure process. The longer-term changes in the device due to shadowing and consequent degradation were demonstrated.

Detailed Discussion of Results

Shadowing Effects on Modules

Our initial work focused on determining if macroscopic defects were responsible for metastability. To pursue that topic we collaborated with Steve Johnston and others at NREL to study full sized and minimodules by electroluminescence and lock-in thermography under current-limited reverse bias conditions. [3, 5, 6] This allowed controlled damage initiation in the modules. Current-voltage curves for the devices were obtained periodically during stressing to demonstrate how the defects formed affected the devices overall. Statistical analysis of the observations allowed a reliable determination of the source of the damage.

Initial measurements showed that there were no macroscopic defects giving rise to metastable behaviors. No large area changes were occurring in a reversible manner under light soaking, allowing us to rule out any obvious manufacturing defect, second phase, or interconnect issue. However, during these measurements we did observe that permanent, irreversible damage was occurring. The remainder of this portion of the work focused on determining the mechanism of that damage.

We observed that as current was allowed to increase under reverse bias, local hot-spots developed. The temperature increased with increasing current, as expected (see Figure 1). When stressed at high currents, permanent damage occurred leading to "worm track" defects spreading out from the point of origin dendritically along a series of paths (rather than along a

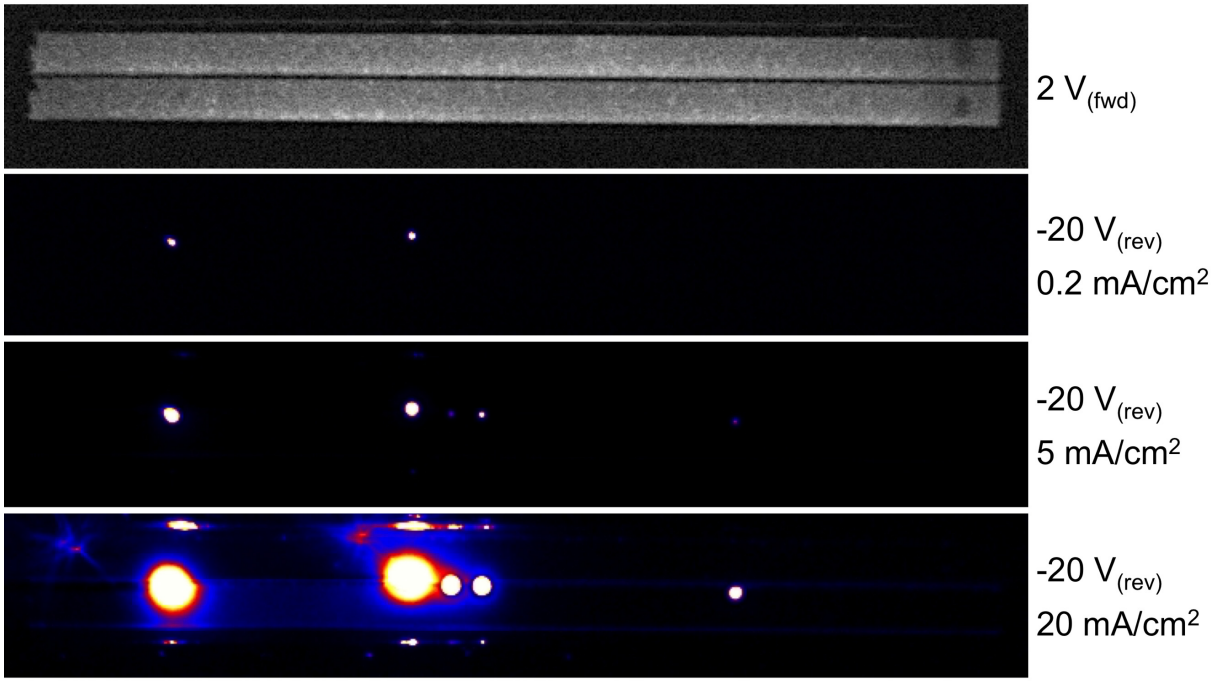

Figure 1: a dark lock-in thermography image of a pair of 4 mm x 85 mm devices interconnected monolithically in forward bias (top) and at -20V with increasing current in reverse bias. Note the uniform heating in forward bias with no visible defects while in reverse bias several distinct hot-spots develop along the interconnect and grow with increasing reverse bias.[3]

single track) (Figure 2). When damage was in progress, successive jumps in current (or reductions in bias voltage) were observed. These jumps appeared to be correlated with individual changes in the worm track defects and led to increased shunt current. The damage is associated with the absorber layer of the device (Fig 2b) primarily rather than the top or bottom contacts. Electron-beam-induced-current (EBIC) measurements show no photocurrent when operated as a photovoltaic at the worm tracks, indicating that these degrade performance to the point of locally destroying the device. Microscopic analysis shows voids in the upper portions of the absorber layer in the damaged regions.

The initiation point of the damage was determined by low-current stressing where hot-spots could be identified without causing changes in the material (Fig 1). We could then perform further analysis at these sites in the scanning electron microscope. The locations of initiation points were found to generally correlate with pinholes in the CIGS absorber layer where the front and back conductors came into contact. Various other defects such as cracks in the absorber layer were also observed as initiation points. This type of defect is part of the reason for improved performance when the heterojunction is produced by chemical bath deposition of CdS, because the CdS adds series resistance to the shunt path. This was originally proposed when it was observed that devices using undoped CdS deposited by conformal coating methods outperformed devices produced by evaporation of highly doped CdS. An example of the changes in current/voltage curves is shown in Figure 3. The damage appears in the form of sudden increases in current through the device under bias due to the shunt.

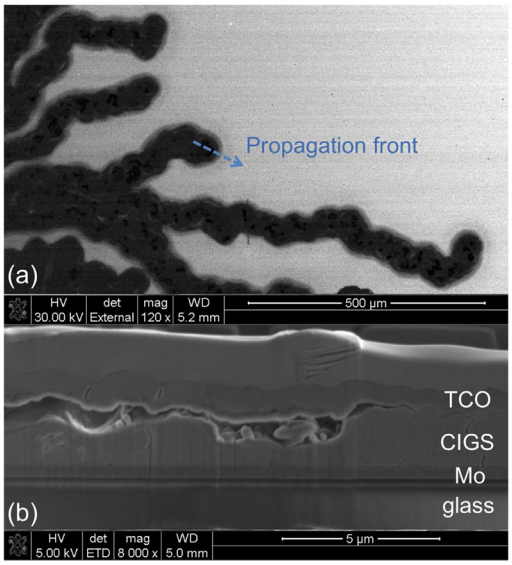

Figure 2: (a) An EBIC image of a worm track defect initiating from a monolithic interconnect showing the propagation along a series of tracks. The dark areas show low or no current collection. (b) A cross-sectional image of a FIB sample showing voids at the CIGS surface in the damaged areas. [3]

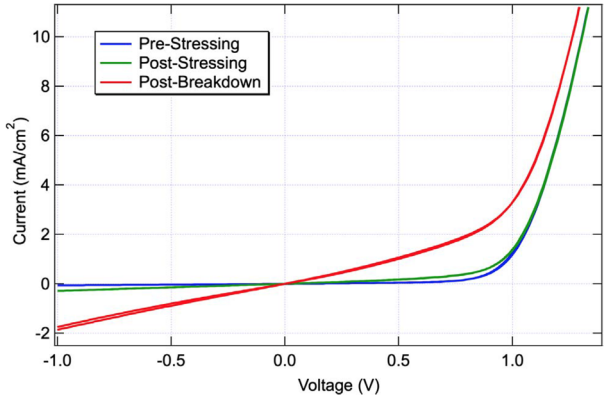

Figure 3 shows the effect of reverse bias damage shown in Fig. 2. The primary damage is shunting.

Metastability due to Point Defects

Solar Cells Measured

(Cu,Ag)(In,Ga)Se_2 solar cells supplied by two manufacturers, Solibro and MiaSole were studied in detail. Both organizations made some changes to their processing. Notably MiaSole was willing to make significant changes in their back contact, absorber deposition conditions, and others. In addition, many specialized devices covering a wider range of processing conditions and compositions were produced at Old Dominion University by the Marsillac group (one of the participating institutions in this collaboration). The ODU samples had energy gaps of ~1.22±0.02 eV, and similar films finished to produce complete solar cells result in very good devices with efficiencies in the range of 17%.

Analytical Techniques Developed

Several analytical techniques were either developed or refined as part of this project. These included a fast C/V analytical method[1], [2] (with the technology established at MiaSole as part of the research), a nanoprobe DLTS method with submicron lateral resolution, and an electron energy loss spectroscopy (EELS) method for measuring defect states in the energy gap of the material.

The fast C/V measurement method was conducted as follows.[7] A capacitance meter with a 100 kHz bandwidth measured capacitance response using a 1MHz, 30mVp-p ac signal. A triangular voltage ramp with a variable ramp rate was applied to the sample using a function generator to provide the voltage. The voltage ramp ran from -1 to 0.3 V. During the ramp the capacitance, conductance, and voltage were recorded so that as the voltage was swept through the triangular cycle the entire voltage range could be measured quickly. Net doping profiles were calculated based on the C/V data following standard methods. As an example of its application, the carrier concentration in the MiaSole samples were measured over a range of depths. In some cases there was significant depth dependence between $2x10^{15}$ to $8x10^{16}$ cm^{-3}, but most values were close to $1x10^{16}$ cm^{-3} with little depth dependence. Fast C/V sweeps the DC voltage fast enough that traps cannot respond (or empty) during the entire measurement. Thus, the extracted doping density in the case of fast C/V is actual acceptor concentration while the doping extracted from the normal C/V is a combination of the acceptor and trap concentrations. In fact, this can be exploited using very slow C/V and fast C/V to subtract the slow C/V extracted doping from the fast C/V extracted doping to estimate the mid-gap concentration with a few minute measurement avoiding the complexities and equipment requirements of DLTS. Additionally, Miasole typically performed C/V measurements at 200 K to slow the trap emission rate, which is another way to extract the true acceptor concentration. However, low temperature C/V is time consuming and requires special equipment and liquid nitrogen. Hence, fast C/V is a fast, cheap, and simple process to extract accurate acceptor concentrations.

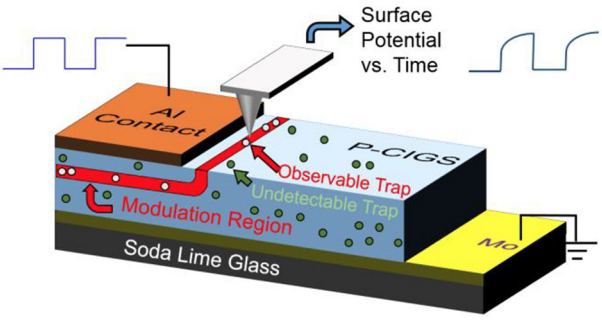

Figure 4: a schematic diagram of the scanning deep level transient spectroscopy method. Figure from Reference [2].

The scanning deep level transient spectroscopy method was developed as part of this project to allow nanometer-scale

mapping of trap concentrations and correlation with local chemical, structural, and electronic characterization in the same exact locations.[8] It is conducted as follows. An Al Schottky contact was applied to the front surface of the CIGS layer with the back Mo acting as an ohmic contact, resulting in a complete diode junction. Surrounding the edge of the Al contact is a depletion region that can be probed as a function of distance from the contact with a scanning Kelvin Probe adaptation of an AFM. This allows determination of the surface potential across the depletion region on the surface of the film. The approach is shown schematically in Figure 4.[2]

The EELS method used here was carried out in a high-performance FEI Titan G2 STEM with a high resolution electron energy analyzer. The energy resolution was 130 meV. Samples were prepared using a FEI Helios focused ion beam system operating with a 30kV Ga ion beam. Following the initial cut the surfaces of the sample were polished with a 5 kV beam to minimize surface damage due to the Ga beam. The primary electron beam in the TEM was had an energy of 60 kV at 30 nA and a 12 mrad beam convergence angle. The transmitted beam was collected over a 22 mrad angle. One of the improvements to the technique demonstrated as part of this project was developing a low-loss measurement that allowed ultra-high energy resolution. The resulting spectra were fit with a triple Gaussian function. This allows separation of three components of the signal, the zero loss electrons that pass through the sample with unchanged energy, electrons that lose energy due to band-to-band transitions in inelastic interactions, and a broad continuum of transitions beyond the band edges. This allows the bandgap profile to be determined at any given position (Figure 5). Subgap absorption can be determined by minor residual components in the signal.[4]

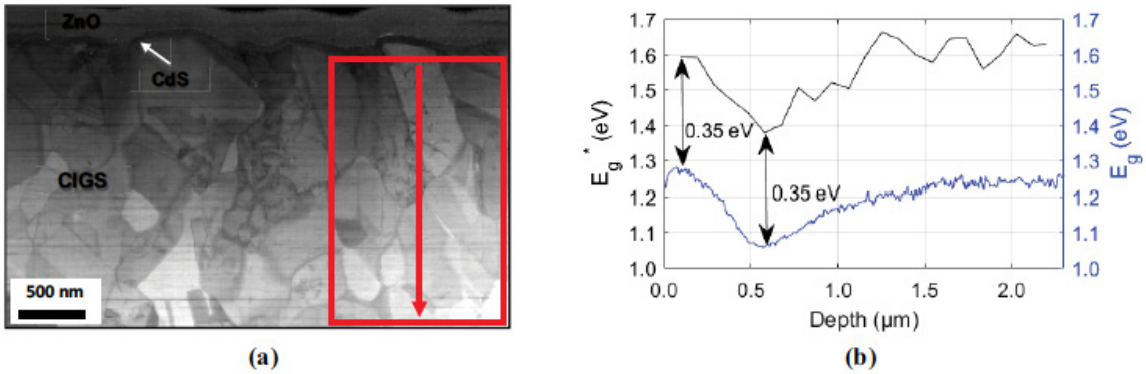

Figure 5: (a) a cross sectional bright field image obtained in the STEM for a CIGS device sample grown at ODU. (b) the band gap profile obtained from the measurement in the STEM (top black curve) and estimated from an energy-dispersive spectroscopy composition profile (bottom blue curve). (Figure from Reference [4])

In addition to the scanning DLTS measurement the basic properties of the CIGS absorber material and the back Schottky barrier were determined by current/voltage (J/V) and capacitance/voltage (C/V) measurements. These showed, for example, that CIGS films grown at ODU for this study had p-type carrier concentrations of $1.2\pm0.1 \times 10^{15}$ cm^{-3} for single stage and three stage deposition processes. Conventional DLTS and DLOS measurements were also made on these devices.

We identified specific nanoscale defects by these methods and compared the results with simulation. The results were correlated with changes in light, bias voltage, processing and humidity. The light induced metastability was correlated with devices made under identical conditions as full scale modules. In the case of MiaSolé modules, these are the same since the modules are constructed from discrete devices.

Observed Behaviors

Two defects were observed in all of the films analyzed, one near midgap and the other near the conduction band edge. [9]

TABLE I
Light-induced changes for the three CIGS samples

	Sample 1	Sample 2	Sample 3
η _change (%)	-0.6	-1.16	-0.6
V_{OC} change (V)	-0.01	-0.02	+0.005
J_{SC} change (mA/cm^2)	**-0.20**	**-0.85**	**-1.25**
FF change (%)	-1.4	-1.8	0.0
[E_V + 0.98 eV] (cm^{-3})	1.5×10^{15}	5.0×10^{15}	6.0×10^{15}
C-V NA change (cm^{-3})	1.0×10^{15}	3.5×10^{15}	5.1×10^{15}
[E_V + 0.53 eV] (cm^{-3})	1.3×10^{13}	2.3×10^{13}	BD
BD = below detection			

The Midgap State

Temperature-dependent DLTS measurements identified a hole trap near midgap (0.43 to 0.56 eV above the valence band). This trap energy varied with CIGS bandgap, but the trap energy with respect to the conduction band was constant at E_C-0.72 eV independent of the bandgap range tested. The concentrations for this defect along with the second at 0.98 eV above the valence band for the Solibro samples are given in Table I. For the ODU material the midgap defect concentration was $2.5\text{x}10^{14}$ cm^{-3}. These midgap trap state densities are below the prevailing carrier concentrations in each sample in all samples studied.

Scanning DLTS measurements place these trap states at or near grain boundaries (Figure 6, in this case in an ODU sample). Similar results were obtained for the other sample sources.

With the DLTS we also determined the cross section for hole trapping to be $1\text{x}10^{-17}$ to $1\text{x}10^{-18}$ cm^2, which is an important input to modeling calculations. The results were directly confirmed by EELS spectral analysis comparing regions with grain boundaries from regions without.

The Near-Conduction-Band State

In addition to the midgap state, a defect state located ~0.98 eV above the valence band was identified by DLOS in samples from all three sources. The concentrations in the ODU samples ranging from $6\text{x}10^{14}$ cm^{-3} to $2\text{x}10^{14}$ cm^{-3} for single and three stage deposition processes, respectively. For the samples from Solibro the values are an order of magnitude greater, approaching the hole concentrations and suggesting a significant amount of compensation in the donor and

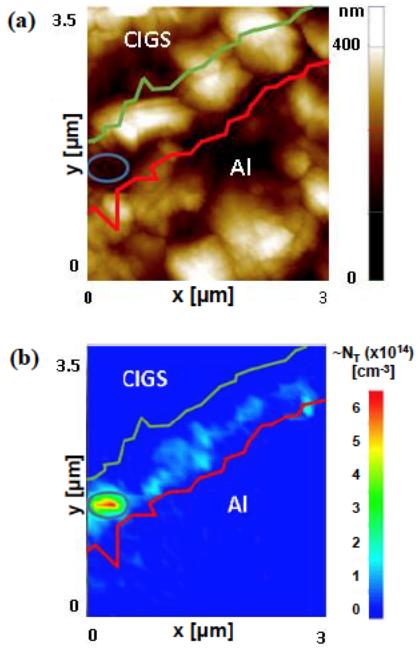

Figure 6: (a) an AFM image of the sample surface showing the two sided of the depletion region (red and green) and the scanning DLTS results (b).

acceptor state populations. Compensation is commonly observed in these materials so a high defect density is not surprising.

Modeling the Defect Behaviors

By comparing the magnitude of the defect concentrations in the MiaSole samples with the performance of the corresponding devices, we find that the midgap (560 meV) defect is correlated with a metastable response in the open circuit voltage (V_{oc}). The 980 meV defect controls metastable response in the short circuit current (J_{sc}).

We simulated the observed behaviors with the numerical computer model SCAPS and other modeling tools and showed that the changes in the specific defect level concentrations are consistent with the observed metastable response in the devices. The loss of current associated with the 980 mV defect is mostly related to a reduction in depletion width and therefore to a lower collection depth. The current lost is restricted to the red portion of the spectrum and is quantitatively linked to the trap occupation. Based on changes in the Se activity tested in samples produced at MiaSole, the trap responsible at 980 meV was concluded to be due to Cu-Se divacancies. This is consistent with the observation that these defects are linked to the valence band states (anion-dominated) rather than to the conduction band (dominated by the group III s-orbital).

Jsc instability

Solibro samples exhibited significant light-induced J_{SC} instability where J_{SC} dropped between 0.2 and 1.25 mA/cm^2 under 1 sun illumination. Figure 7 shows the impact of light where the EQE showed a drop is long wavelength collection after light soaking. [1]

To understand what role defects might have, DLTS and DLOS were performed with results shown in Figures 8 and 9.

There is a clear correlation between the E_V+0.98 eV trap concentration and the J_{SC} instability, but no correlation with the E_V+0.53 eV trap. The acceptor concentration in these films was only ~1x10^{15} cm^{-3}, so the E_V+0.53 eV trap is significantly smaller than the doping while the E_V+0.98 eV trap concentration is several times the doping concentration. The solar spectrum contains light with energy above 0.98 eV, which empties the E_V+0.98 eV trap over time meaning the effective acceptor concentration increases from 1x10^{15} cm^{-3} in the dark up to 6x10^{15} cm^{-3} in light. This large change in effective doping, which is proportional to the trap concentrations in Fig. 8, was analyzed at CSM and OSU and revealed the mechanism of light-induced J_{SC} reduction.

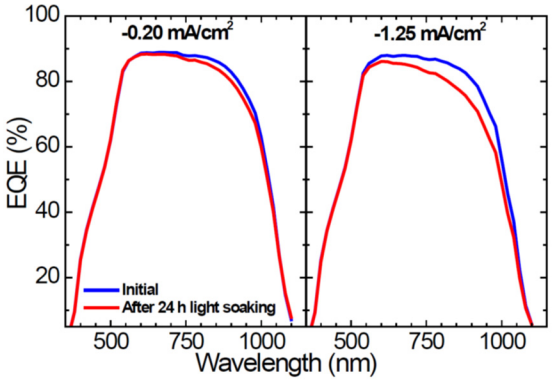

Figure 7: EQE spectra before and after light soaking (left) Sample 1 (-0.20 mA/cm^2) with the lowest instability and (right) Sample 3 (-1.25 mA/ cm^2 J_{SC} degradation) with the highest instability. Larger reduction in EQE is observed in the long wavelengths of Sample 3, consistent with the J_{SC} degradation and indicating the CIGS layer is responsible for the J_{SC} reduction. [1]

The E_V+0.98 eV trap emitted under 1 sun illumination, that increased the effective acceptor doping, and that reduced the depletion depth, which reduced the carrier collection at longer wavelengths. A reasonable metric for the impact of this effect will be is the concentration of the E_V+0.98 eV trap relative to the doping concentration. The larger the ratio the larger the light-induced J_{SC} reduction.

V_{OC} instability

The Miasole cells did not suffer from much light-induced JSC instability (<0.3 mA/cm^{-3}) but did have light-induced VOC instability ranging from +13 mV to -35 mV as shown in Table II.

TABLE II: LIGHT-INDUCED CHANGES IN CIGS SOLAR CELL PARAMETERS AND RESULTS OF MODELING FOR COMPARISON.

	Sample 1	Sample 2	Sample 3
	Experimental results		
η change (%)	-1.27	-0.30	+0.27
V_{OC} change (mV)	**-35**	**-9**	**+13**
J_{SC} change (mA/cm^2)	-0.2	-0.1	-0.02
FF change (%)	-1.4	-1.8	0.0
	TCAD modeling results		
V_{OC} change (mV)	**-24**	**-13**	**+8**
J_{SC} change (mA/cm^2)	-0.2	-0.3	-0.3
FF change (%)	-2.0	-1.7	-0.5

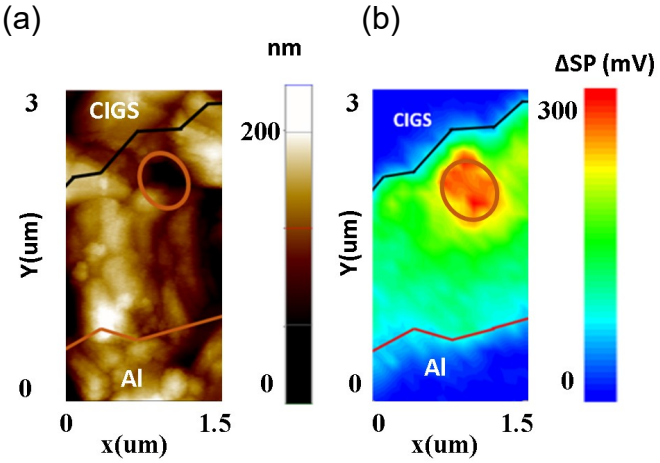

Figure 10. Scanning-DLTS map for sample 1 shows that the E_V+0.57 eV trap is not spatially uniformly distributed. Comparing the trap image (b) with the topography image (a), the E_V+0.57 eV trap is mostly distributed in some grain boundary region.

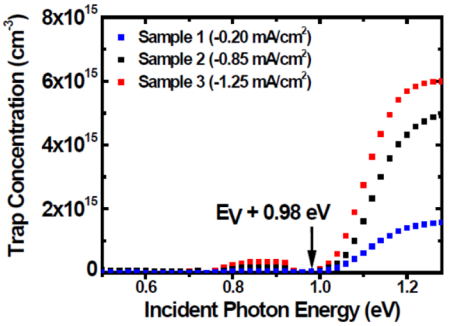

Figure 8: DLOS steady state photocapacitance spectra showing a correlation between the E_V+0.98 eV concentration and J_{SC} reduction.

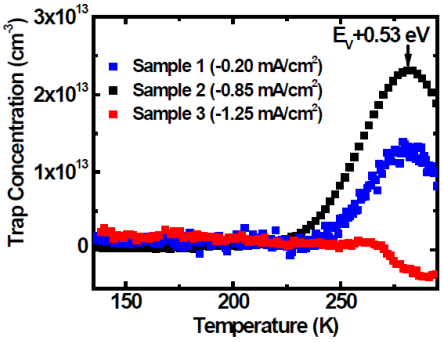

Figure 9: DLTS spectra showing trap with activation energy E_V+ 0.53 eV. Concentration of E_V+0.53 eV shows no correlation with J_{SC} reduction indicates E_V+0.53 eV might not be the cause of J_{SC} reduction.

The issue was much more complex than the J_{SC} instability issue. Here, multiple traps were involved. The E_V+0.98 eV trap emitted under light, which led to an increased effective acceptor concentration, just like the J_{SC} instability discussion. The increased doping enables more Fermi level splitting and increased V_{OC} given by

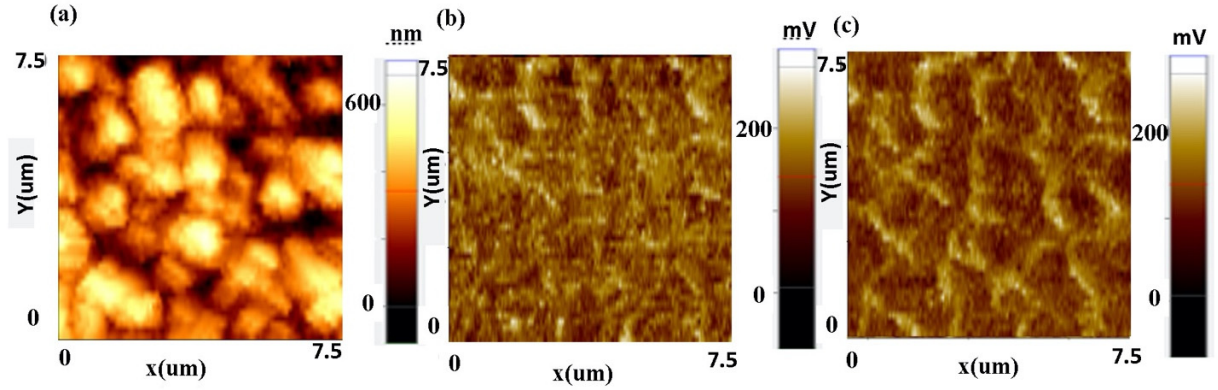

Fig. 11. (a) AFM topography, (b) SKPM image with the pre-light-soaked condition, and (c) SKPM image after light-soaked conditions of the same region of bare CIGS for Sample 1 in the same physical locations for each image.

$$\Delta V_{OC} \sim kT \ln\left(\frac{N_{A,light}}{N_{A,dark}}\right) \qquad (1)$$

So the E_V+0.98 eV trap always causes an increase in V_{OC} under illumination because the doping under illumination is always higher than in the dark. However, the midgap E_V+0.57 eV trap acts as a recombination center that tends to reduce V_{OC}. It always acts as a recombination center whether in the light or not, so this itself would not lead to a light related V_{OC} change. However, the E_V+0.57 eV trap is located at specific grain boundaries (Figure 10) and under illumination Figure 11 shows that the grain boundaries exhibit band bending under illumination where the bands bent such that E_F-E_V increased ~55 mV. This leads to more electrons at the grain boundaries on average and enhances the recombination. DLTS and DLOS are shown in Figures 12 and 13 where the E_V+0.57 eV, unlike the E_V+0.98 eV trap, shows a clear dependence between the trap concentration and how negative the light-induced V_{OC} change in Table II is.

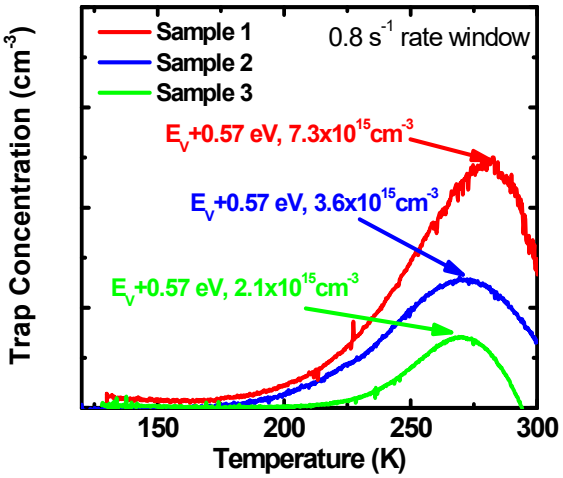

Fig. 12. DLTS spectra for all three samples using a 10 ms fill pulse at +0.2 V and measurement at -1.0 V. An E_V+ 0.57 eV trap is observed in all three samples whose concentration correlates with the V_{OC} instabilities listed in Table II.

To bring all this together in an understandable and quantifiable way, two dimensional TCAD simulations were used to quantify all the experimental observations. The simulation began by fitting the EQE to match the J_{SC} and the initial trap concentration used to match the cell parameters. Then to model the impact of the light, the emitted E_V+0.98 eV traps were simulated with extra acceptor charge added to the CIGS and band bending at the grain boundaries by reducing the acceptor concentration locally. No parameters other than this were varied to extract the light-induced changes in the simulations. The results are shown in Table II where qualitatively we can simulate the positive and negative light-induced V_{OC} changes.

Quantitatively, we see close correlation between the experimental and simulation data in Table I indicating the observations and conclusions are likely on target. This indicates that two traps likely determine the light-induced V_{OC} instability and control of both traps is necessary to mitigate cell to cell variability and reduce the gap between cell and module efficiencies.

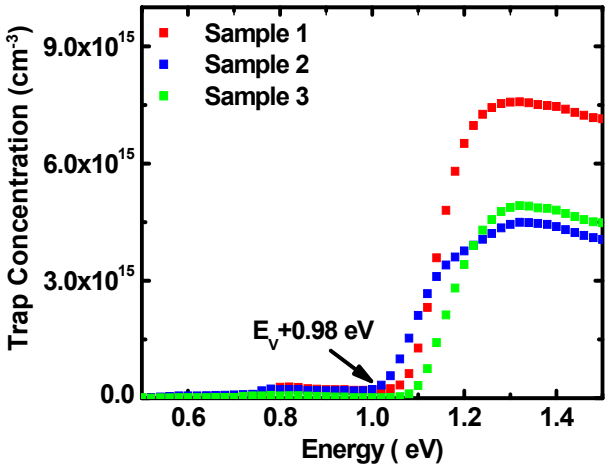

Fig. 13. Comparison of steady-state DLOS spectra using a 10 s fill pulse at +0.2 V and measurement at -1.0 V. One defect is observed with an energy of ~Ev+0.98 eV.

Impact of Dry Heat

We also investigated the role of dry heat on the trap densities. Figure 14 shows the defect spectroscopy results. After 1000 h at 85 °C in encapsulated packages to minimize any humidity effects, we observed decreases in both the E_V+0.98 eV and E_V+0.59 eV trap concentrations. This was the first mechanism we observed to significantly reduce the midgap trap concentration, which is a promising step as this level as a midgap trap is an efficient recombination center as shown in the V_{OC} instability study and mitigating this level is critical to reduce the V_{OC} deficit ($E_G/q - V_{OC}$).

Alkali Metal Effects (Rb, K, and Na)

We have studied the effects of alkali metals on the metastable response of the devices and on the defects identified above. [10-14] We have produced samples with and without Na post-deposition treatments at Old Dominion. For the Na doped sample, the activation energy of the observed trap was slightly smaller (i.e., shallower) at E_V + 540 meV. The small difference in energy is likely the result of the slight compositional differences between the two samples and bandgap gradient throughout the sample rather than a fundamental difference in the nature of the traps. The midgap trap concentration, ~2.5x10^{13} cm^{-3}, was found to be nearly identical between the two samples indicating that this trap is not sensitive to Na doping.

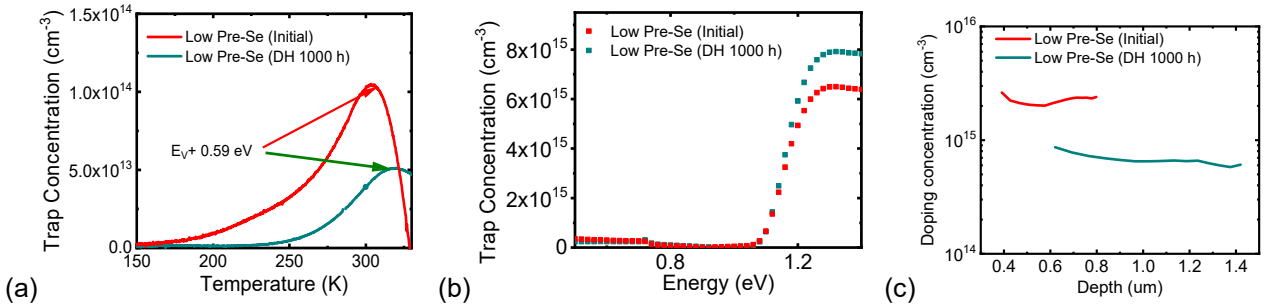

Figure 14: (a) DLTS spectra showing the E_V+0.59 eV trap decreasing by a factor of ~2 after 1000 h of dry heat stress. (b) DLOS spectra showing the E_V+0.98 eV trap increasing after dry heat. (c) Doping profiles from fast capacitance-voltage measurements (2000 V/s sweep rate) before and after 1000 h of dry heat stress. Dry heat leads to a ~1-1.5x10^{15} cm^{-3} reduction in the net acceptor doping, which will lower V_{OC}.

The Na-doped sample exhibits a ~4X reduction in the 980 meV trap concentration, showing that Na is responsible for passivation of the 980 meV level. Therefore, we have concluded that the 980 meV level resulting in current metastability is reduced by post-deposition treatment with Na. This is also true of Na added during material growth. Modeling the expected effects of the 980 meV trap concentration on J_{SC} in these samples shows that it is negligible at the lower defect concentration in the presence of Na. Nonetheless, the 980 meV trap does play a role in the cell properties by changing the effective doping in the material and thus the depletion depth changes.

We have quantitatively connected the doping change to the trap and to the change in photocurrent collected and thus verified the conclusion by numerical simulation. We note however that simulation shows that there are many parameters that interact in this conclusion and that sodium's impact on cell performance is quite complex and varied from sample to sample depending on the doping, diffusion lengths, and trap concentrations. Furthermore, sodium can diffuse under high temperature or electric fields, so we expect the module service lifetimes will be sensitive to the Na or K concentrations.

The detail of analysis we have conducted is definitive about the sources of metastability but is difficult to perform even on selected samples from a production process. Therefore we are looking for both process conditions that affect metastable response as well as analysis methods that are quick and easy to perform that would give a measure of the expected metastable response.

We examined the effect of selected process condition changes, driven by our earlier results based on material produced at MiaSolé. We received a number of samples processed with different conditions and material compositions and which show different metastable responses. We have demonstrated clear differences in the x-ray diffraction patterns for the samples that are correlated with the organization of point defects. For example, we have shown that the addition of Ag to the absorber material narrows the diffraction peaks, consistent with better organization of atoms in the crystal structure and hence to fewer point defects. This is also consistent with our earlier studies of $AgInSe_2$ single crystal epitaxial layers.[15]

We have studied the effects of water exposure of various layers in CIGS devices on final device properties and performance as described in later sections of this report. Here we focus on the effects on defect states in the energy gap of the CIGS. Exposure of the device during most phases of deposition has limited effects, described below. Water exposure of the CIGS itself has a significant negative impact on device performance and in particular increasing both the 980 meV and 560 meV defect densities.

Raman Spectroscopy for Analysis of Metastability

A convenient opportunity to study metastable light-induced changes in CIGS solar cells is to look for changes in the Raman spectrum as a function of time during the measurement, since Raman intrinsically requires moderately intense near-band-gap light exposures. We observed consistent and significant changes to the Raman signal in (Ag,Cu)(In,Ga)Se_2 [ACIGS] absorber layers fabricated as complete solar cells at MiaSole.[16]

The samples covered a variety of processing conditions comparing with and without added Ag, with and without Na and K and when and how these were provided to the samples. In addition the Mo back contact was pre-treated with Se in some cases. X-ray diffraction data showed the effect of composition gradients on the lattice constant of the films and generally showed the material to be high quality polycrystalline ACIGS with little texture. Chemical differences associated with Ag addition were reflected in the peak positions but the overall crystallinity was effectively unchanged.

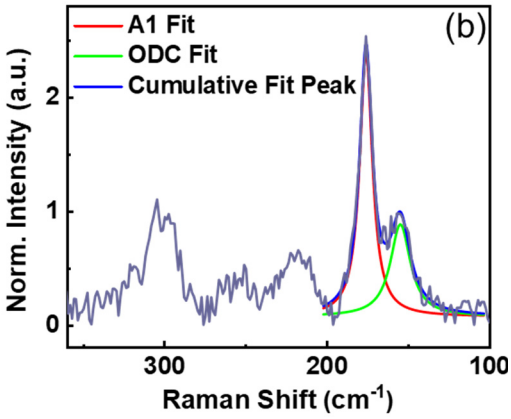

Figure 15: A typical Raman spectrum from the MiaSole ACIGS material showing the peaks from left to right due to CdS, group III related vibrations (two peaks) and the A1 (Cu-Se) and ODC vibrational modes with corresponding peak fits.

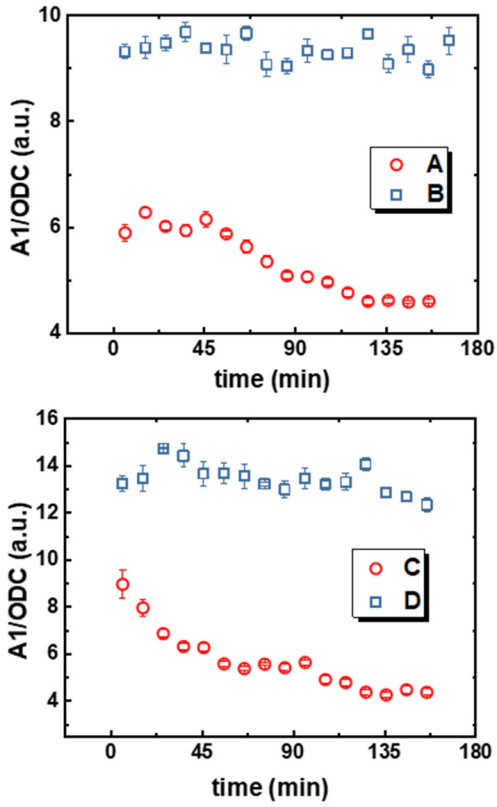

Figure 16: The A1/ODC Raman mode trend with time for several ACIGS samples produced at MiaSole.

Raman peaks were observed and identified as follows (example spectrum in Figure 15). A peak at ~303 cm^{-1} was concluded to be due to CdS and showed no changes under light exposure. It was used as an intensity reference for comparison among spectra. Raman modes at 177, 219, and 258 cm^{-1} were concluded to be the A1, B2 and E modes, respectively. The B2 and E modes showed little change in intensity or position under extended illumination. These are primarily associated with vibrational modes due to the group III element. The 177 cm^{-1} mode is generally associated with the Cu-Se bond vibrations. It showed large changes in intensity relative to the CdS mode from sample to sample and with illumination time. In addition, a mode at 156 cm^{-1} was concluded to indicate an ordered

defect (ODC) structure. In general, the intensity of this ODC mode was inversely related to the 177 cm^{-1} mode.

Light exposure produced consistent changes in the peak intensities of the 177 and 156 cm^{-1} modes that varied over time as shown in Figure 16. In the data shown in that figure the A1/ODC ratio was relatively low and decreasing for samples deposited with K added to the Mo back contact and with a decreasing Cu/III ratio near the sample surface (verified by SIMS analysis). The higher and more stable peak ratios were consistent with higher Cu near the film surface.

In a different set of samples the A1 and ODC peak intensities were studied as a function of processing conditions. The results are shown in Figure 17.

The Raman results indicate a consistent behavior independent of growth temperature but with a significant trend to lower ODC signal without added K or with lower pre-selenization of the Mo.

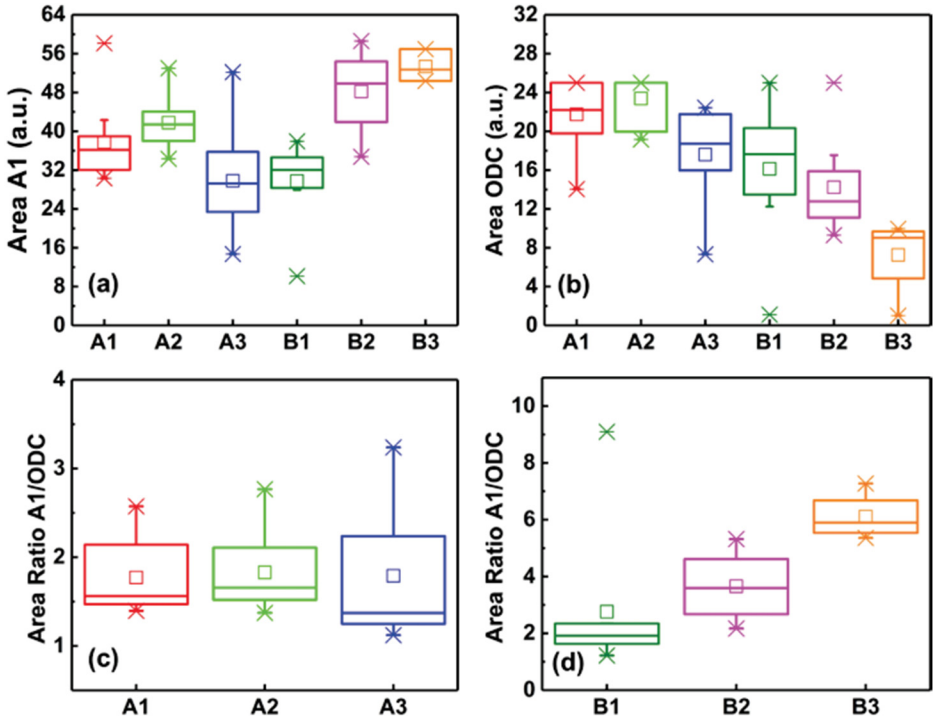

Figure 17: The A1 and ODC peak areas and area ratios for samples from group A (growth temperature varied) and group B, varying the selenization of the Mo back contact prior to CIGS deposition and without added K (sample B3).

Effects of Water Exposure on Devices

A systematic approach to analysis of the effects of water exposure on devices was undertaken. [11, 17-22] [23] In this study devices were synthesized at Old Dominion University by the Marsillac group and tested for performance. The performances of baseline devices were found to be consistent from one measurement to the next. The synthesis process was interrupted between different layers in some experiments and the structure at that point was soaked in deionized water. The devices had no intentional addition of Na so the only source was the soda-lime glass underlying the Mo.

Figure 18 shows box plots of device performances as a function of water exposure at various stages of the synthesis. The j/V curves were analyzed to determine the properties of each individual diode dark current (J_0), ideality factor (a), and shunt and series resistances.

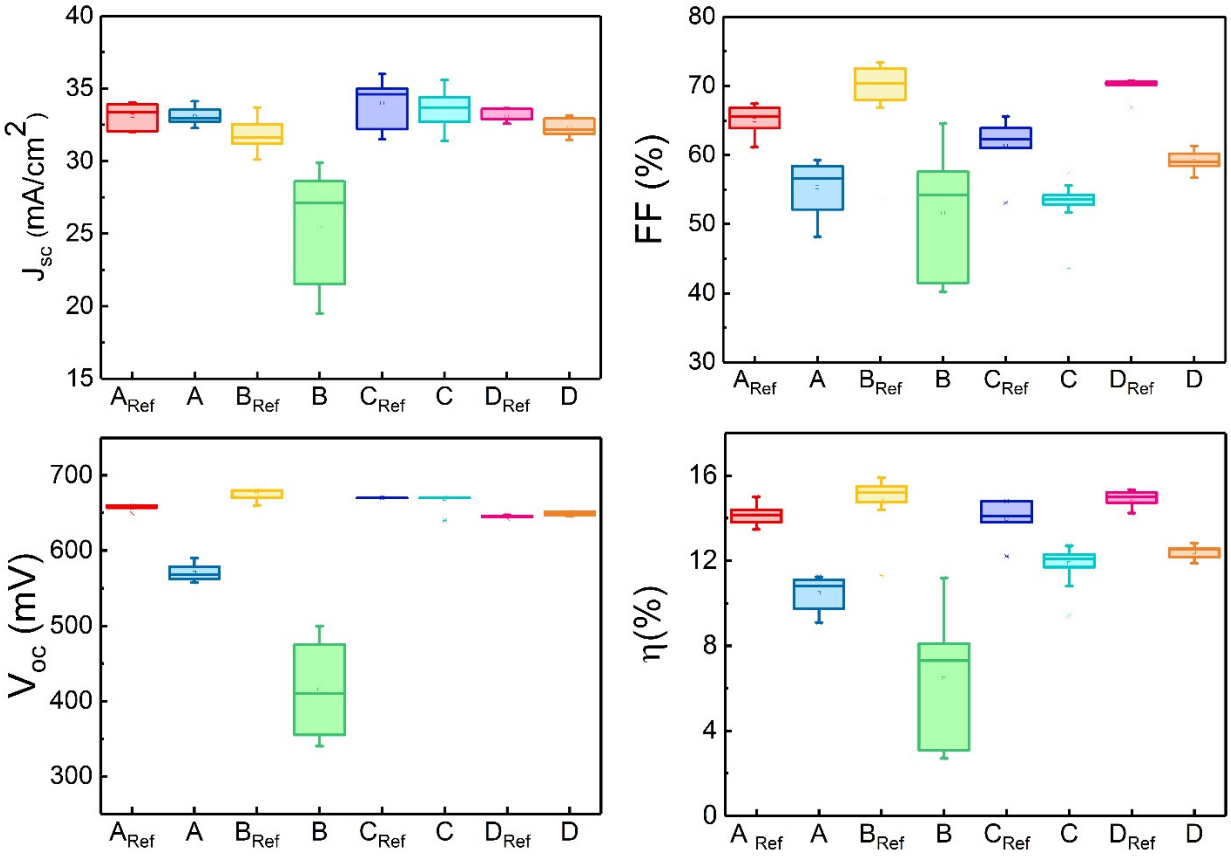

Figure 18: Box plots of device performances for the typical parameters, open circuit voltage (V_{oc}), short circuit current (J_{sc}), fill factor (FF), and efficiency resulting from water exposure between the Mo (sample A) and CIGS (sample B) and CdS (sample C) and the transparent conducting oxide (aluminum-doped ZnO or AZO). The corresponding performances of samples produced concurrently but not exposed to water are the reference values.

Water soaking between the Mo and CIGS layers resulted in an increase in J_0 by a factor of 10 on average and a modest increase in shunt current. This resulted in a decrease in fill factor due to the shunt and a decrease in V_{oc} due to the increase in J_0. The change in J_0 was attributed

primarily to removal of Na from the Mo layer and consequently from availability during the CIGS deposition. It is well known that Na improves V_{oc} by reducing point defects. The increase in shunt current presumably resulted from handling during water exposure.

The major reduction in performance resulted from water soaking after the CIGS deposition and before the CdS. This caused an increase in J_0 by a factor of 100, an increase in ideality factor and in shunt current. The result was a loss of performance in all parameters. In some respects it is surprising that water soaking would have degraded the performance so much at this stage, since the CdS chemical bath deposition process is based on an aqueous solution at an elevated temperature. Therefore the chemical bath deposition process results in water exposure of the CIGS surface. It is possible that the various solutes, particularly various ions in the solution reduces damage to the CIGS surface. However, previous studies show no significant impact of partial electrolyte treatment on the device. We conclude that it is not dissolution or oxidation of the CIGS surface in the short term that is responsible for this change. Rather it is presumably the longer-term exposure that is the issue. We anticipate that the damage is the result of degradation of the CIGS surface over time in the same way that CIGS devices perform best when they are coated with CdS as soon after deposition as possible, potentially avoiding air exposure entirely.

Water soaking after the CdS results in a reduction in fill factor, primarily due to an increase in series resistance. There was a small decrease in J_{sc} but the majority of the change was in fill factor. There was almost no change in the behavior of the diode properties themselves. The reduction in J_{sc} was across the spectrum based on external quantum efficiency (EQE) measurements, suggesting a change in reflection or an overall failure to collect charge at the heterojunction. This result is consistent with the observation that CIGS devices, once coated with CdS, are relatively stable.

Finally, water soaking of the aluminum-doped ZnO transparent conductor (AZO TCO) results in a decrease in fill factor resulting from a significant increase in series resistance and a decrease in shunt resistance. There was no significant change in the diode properties, although some light soaking changes develop as a result of this water soaking. These observations are less significant that were anticipated as there has been discussion in the literature that the primary problem with failure of edge seals in CIGS device encapsulation is degradation of the AZO TCO. The increase in series resistance is expected if there is some loss of conductivity due to damage of the AZO.

Water exposure of the Mo surface before CIGS deposition has subtle effects on the device but overall degrades performance. It results in an increased depletion width and decreased doping level, potentially correlated with a modest decrease in alkali metal concentrations in the Mo and CIGS. It leads to a decrease in V_{oc}, and a slight decrease in photocurrent in the red portion of the spectrum. In addition, the diode behavior results in an increased reverse saturation current.

Water exposure of the CdS and ZnO layers had no obvious effect on the device itself, although the series and shunt resistances were impacted, possibly simply because of the additional handling of the devices.

Discussion

The Midgap State

We were unable to establish a clear cause for the midgap states, which is significant because these should be the most active recombination sites for carriers. However, we can make some

observations. There are two strong candidates in our opinion for the midgap state. The I on III antisite defect and dangling bonds.

The argument for the antisite defect is as follows. The defect is located primarily at grain boundaries and is present at relatively low concentrations. In some cases, we have observed a higher Cu and reduced group III content in the boundaries where the trap was found. Excess S was also detected in these locations but the trap state has been observed in materials that had never been exposed to S so we do not believe the trap to be associated with S. The I on III antisite defect should be sufficiently common in these materials. The phase diagram shows a chalcopyrite to sphalerite (disordering of the cation sublattice) at temperatures moderately above the growth temperature and in group III rich material, such as is used in devices. The I on III antisite defect is a divalent substitution so one would expect two defects to be present. A hydrogenic model would put the doubly-ionized state roughly four times deeper in the gap than the singly-ionized defect. In studies of single crystal CIGS grown at high temperatures where the tendency to disorder the cation sublattice should have been higher, the Rockett group observed a dominant acceptor at ~160 meV depth[24] that was unaffected by Na, although a compensating donor, possibly the divacancy, was reduced by Na.[25] This would have been the singly-ionized acceptor so a much deeper acceptor in the energy range of the midgap state would be reasonable to expect. The concentration of these defects would also be consistent with the observed density of defects in the films. Finally, the antisite defect would potentially track the valence band edge. The defect observed by the Rockett group had essentially the same ionization energy independent of Ga content in the film[24] so it was presumably derived from a valence band state. Thus, there is a reasonable argument to be made that the deep state is the I on III divacancy.

The primary argument against the I on III antisite defect is that it should be doubly ionized and hence would require a large donor population to be present and that the Fermi energy should lie near midgap to ionize it. Because a large amount of band bending is not found at grain boundaries in CIGS typically this seems less likely. Nonetheless, we consider this defect to be a strong candidate for the deep state.

The other reasonable assignment of the defect is dangling bonds in the grain boundaries. CIGS strongly prefers the close-packed (112) surfaces,[26] which should have a single dangling bond per atom. However, to reduce the energy of that surface to the point of being favorable there should be some form of reconstruction, to date not determined, that would further reduce the electrical activity of these dangling bonds to a concentration consistent with the observed density. We can provide a "back-of-the-envelope" calculation related to the density of these defects. We observe roughly $2x10^{14}$ cm^{-3} midgap states and these are associated with grain boundaries. If we model the microstructure as a collection of one cubic micron cube-shaped grains then there would be 10^{12} grains cm^{-3}. Approximating the bulk density as $5x10^{22}$ atoms/cm^{-3} and the surface site density as $5x10^{14}$ cm^2 we can estimate that each cube would have $5x10^{10}$ bulk atoms and $3x10^7$ surface atoms per cubic grain. This would correctly yield $5x10^{22}$ cm^{-3} bulk atoms and $3x10^{19}$ cm^{-3} surface sites. Our measured midgap state concentrations would be one site in 100,000 if distributed evenly. CIGS is known to have strongly passivated surfaces but very clean surfaces have been shown to have their Fermi energy close to midgap.[27, 28] One reasonable explanation is that these states are due to dangling bonds. The very low density of states observed would suggest a very low dangling bond density, indicating that most grain boundary dangling bonds are passivated. However, it would be reasonable to associate the few

remaining sites with occasional unpassivated dangling bonds. This explanation is also consistent with hypotheses that post-deposition treatments can reduce the density of grain boundary defects. There does not seem to be a clear connection of these rare grain boundary defects with any impurity, although at the observed defect density it would be difficult to detect such impurities, even with an atom probe. The argument that the midgap states are due to dangling bonds is also consistent with the observation that alkali metals do not have a strong effect on their density since nearly all grain boundary dangling bonds would have to be passivated somehow in any case.

The density of the midgap states is 0.1 to 1% of the bulk hole density, which would suggest that they would have a relatively minor effect on local doping and would not cause significant depletion at the grain boundaries, as is typically observed. Their variation in density from grain boundary to grain boundary is consistent with an unpassivated dangling bond hypothesis as different grain boundary configurations would be expected to have different surface structures, and surface step and step kink densities. These effects would also explain the variation in observations of grain boundary potentials using scanning Kelvin probes and other methods, which variously report no or modest potential variations at the grain boundaries. If one measures a grain boundary potential in an area of high concentration of midgap states one might expect a high potential change while the majority of well-passivated boundaries would show little or no potential variation.

Finally, the observation that the midgap state primarily affects V_{OC} is consistent with it being a deep hole trap. As such it would have a strong effect on minority carrier recombination. The observed cross sections are two orders of magnitude below the size of an atom, which suggests that the traps tend to be relatively repulsive to holes, suggesting that the defects are normally positively charged. This would promote trapping of minority electrons. The traps would tend to pin the electron quasi-Fermi level as a result, which would be consistent with the observation that the temperature-dependent V_{OC} measurements are linear with temperature and extrapolate to the absorber energy gap down to T~220 K but at lower temperatures the extrapolation is to a lower value. This suggests that as the quasi-Fermi level for holes rises in the energy gap at lower temperatures, that eventually it is influenced by this pinning behavior.

Modeling of the effect of this defect is more difficult because it is variable in density and located at grain boundaries. Therefore, a model would need to account for both of these. Even 2d or 3d models would not account well for the grain-to-grain variations in defect density.

The Near-Conduction-Band state

There is less to say about the E_V+0.98 eV state as its behavior is both more clear and more controllable. It appears to vary with processing and increasing the Se activity, consistent with the Cu-Se divacancy explanation. It is affected by alkali metals, which suggests a mechanism for improvement of device performance – that the alkali metal treatment reduces the divacancy density. The modeling shows that the effect of the defect is straightforward, changing the depletion width and hence the carrier collection behavior in the device.

Conclusions

We consider that this project established the following.

First that there is relatively little effect of direct water exposure on CIGS devices, although extended water soaking can reduce the performance, especially when the surface of the Mo and CIGS are exposed. However, none of these appears to be the cause of degradation of the completed and encapsulated device. Therefore CIGS should be considered to be relatively resistant to damage due to water exposure.

Second that there is a defect, probably the divacancy, that produces a state ~980 meV above the valence band in CIGS and is affected by the presence of Na. This may well be the donor that was reduced in the studies of epitaxial layers so it probably is not directly associated with grain boundaries, as observed here.

Third, there is a deep trap state near midgap that is not affected by Na. This state may be the I on III antisite defect or may be a dangling bond state. Resolution of that question will await results of a follow-on project.

The project accomplished a number of things in addition to these three points. The metastability in CIGS modules was shown not to be due to any macroscopic defect or non-uniformity that might be associated with a manufacturing defect. Several novel materials analysis techniques were demonstrated. Time and light-dependent changes in the Raman spectrum of the material were observed. Scanning probe measurements were applied to CIGS and CdTe. While several of the collaborating CIGS manufacturers went out of business either during the project or shortly after its termination, the project made a strong effort to transfer the technology to the manufacturers that were active at the time and we continue to work with the remaining CIGS manufacturers and the broader CIGS community.

In summary, the project accomplished the goals it set out to determine the sources of metastable device performance, although work remains to establish methods to control the deep defect and to verify the source of the primary defects.

Publications & Presentations:

The project resulted in a number of publications, which are cited in the references below. Overall the publications and presentations of the work are as follows:

June 2016: IEEE PVSC (3 papers & presentations): [21, 22, 29]

February 2016: Presentation at the Module Reliability Workshop, Lakewood CO

June 2017: IEEE PVSC (9 papers & presentations): [1, 2, 5, 7, 9, 14, 20, 30, 31]

June 2018: IEEE PVSC (6 papers & presentations): [4, 6, 12, 16, 18, 19]

June 2019: IEEE PVSC (2 papers & presentations): [10, 32]

Advanced Energy Materials: [8]

Journal of Photovoltaics: [10, 11, 13, 17]

Solar Energy: [3]

References

[1] P. K. Paul, T. Jarmar, L. Stolt, A. Rockett, and A. R. Arehart, "Role of Ev+0.98 Ev trap in light soaking-induced short circuit current instability in CIGS solar cells," in *2017 IEEE 44th Photovoltaic Specialists Conference (PVSC), 25-30 June 2017*, Piscataway, NJ, USA, 2017: IEEE, in 2017 IEEE 44th Photovoltaic Specialist Conference (PVSC), pp. 301-23, doi: 10.1109/PVSC.2017.8366748. [Online]. Available: http://dx.doi.org/10.1109/PVSC.2017.8366748

[2] P. K. Paul, K. Aryal, S. Marsillac, T. J. Grassman, S. A. Ringel, and A. R. Arehart, "Identifying the source of reduced performance in 1-stage-grown Cu(In,Ga)Se2 solar cells," in *2017 IEEE 44th Photovoltaic Specialists Conference (PVSC), 25-30 June 2017*, Piscataway, NJ, USA, 2017: IEEE, in 2017 IEEE 44th Photovoltaic Specialist Conference (PVSC), p. 4 pp., doi: 10.1109/PVSC.2017.8366869. [Online]. Available: http://dx.doi.org/10.1109/PVSC.2017.8366869

[3] E. Palmiotti *et al.*, "Identification and analysis of partial shading breakdown sites in CuInxGa(1-x)Se2 modules," (in English), *Solar Energy,* vol. 161, pp. 1-5, Feb 2018, doi: 10.1016/j.solener.2017.12.019.

[4] J. I. Deitz *et al.*, "Nanoscale Electronic Structure Characterization in CIGS with Electron Energy-Loss Spectroscopy," in *2018 IEEE 7th World Conference on Photovoltaic Energy Conversion (WCPEC) (A Joint Conference of 45th IEEE PVSC, 28th PVSEC & 34th EU PVSEC), 10-15 June 2018*, Piscataway, NJ, USA, 2018: IEEE, in 2018 IEEE 7th World Conference on Photovoltaic Energy Conversion (WCPEC) (A Joint Conference of 45th IEEE PVSC, 28th PVSEC 34th EU PVSEC), pp. 3914-17, doi: 10.1109/PVSC.2018.8547398. [Online]. Available: http://dx.doi.org/10.1109/PVSC.2018.8547398

[5] S. Johnston *et al.*, "Identifying Reverse-Bias Breakdown Sites in CuInxGa(1-x)Se2," in *2017 IEEE 44th Photovoltaic Specialists Conference (PVSC), 25-30 June 2017*, Piscataway, NJ, USA, 2017: IEEE, in 2017 IEEE 44th Photovoltaic Specialist Conference (PVSC), pp. 1400-4, doi: 10.1109/PVSC.2017.8366755. [Online]. Available: http://dx.doi.org/10.1109/PVSC.2017.8366755

[6] S. Johnston *et al.*, "Thin-Film Module Reverse-Bias Breakdown Sites Identified by Thermal Imaging," in *7th IEEE World Conference on Photovoltaic Energy Conversion, WCPEC 2018, June 10, 2018 - June 15, 2018*, Waikoloa Village, HI, United states, 2018: Institute of Electrical and Electronics Engineers Inc., in 2018 IEEE 7th World Conference on Photovoltaic Energy Conversion, WCPEC 2018 - A Joint Conference of 45th IEEE PVSC, 28th PVSEC and 34th EU PVSEC, pp. 1897-1901, doi: 10.1109/PVSC.2018.8547766. [Online]. Available: http://dx.doi.org/10.1109/PVSC.2018.8547766

[7] P. K. Paul, J. Bailey, G. Zapalac, and A. R. Arehart, "Fast C-V method to mitigate effects of deep levels in CIGS doping profiles," in *2017 IEEE 44th Photovoltaic Specialists Conference (PVSC), 25-30 June 2017*, Piscataway, NJ, USA, 2017: IEEE, in 2017 IEEE 44th Photovoltaic Specialist Conference (PVSC), pp. 2414-18, doi: 10.1109/PVSC.2017.8366494. [Online]. Available: http://dx.doi.org/10.1109/PVSC.2017.8366494

[8] J. I. Deitz *et al.*, "Direct nanoscale characterization of deep levels in AgCuInGaSe2 using electron energy-loss spectroscopy in the scanning transmission electron microscope," *Advanced Energy Materials,* vol. 9, no. 35, p. 1901612 (8 pp.), 2019, doi: 10.1002/aenm.201901612.

[9] P. K. Paul, K. Aryal, S. Marsillac, S. A. Ringel, and A. R. Arehart, "Impact of the Ga/In ratio on defects in Cu(In,Ga)Se2," in *2017 IEEE 44th Photovoltaic Specialists Conference (PVSC), 25-30 June 2017*, Piscataway, NJ, USA, 2017: IEEE, in 2017 IEEE 44th Photovoltaic Specialist Conference (PVSC), p. 4 pp., doi: 10.1109/PVSC.2017.8366513. [Online]. Available: http://dx.doi.org/10.1109/PVSC.2017.8366513

[10] S. Karki *et al.*, "Analysis of Recombination Mechanisms in RbF-Treated CIGS Solar Cells," *IEEE Journal of Photovoltaics,* vol. 9, no. 1, pp. 313-18, 01/ 2019, doi: 10.1109/JPHOTOV.2018.2877596.

[11] S. Karki *et al.*, "Degradation Mechanism in Cu(In,Ga)Se2 Material and Solar Cells Due to Moisture and Heat Treatment of the Absorber Layer," *IEEE Journal of Photovoltaics,* vol. 9, no. 4, pp. 74-9, 07/ 2019, doi: 10.1109/JPHOTOV.2019.2912707.

[12] S. Karki, P. Paul, G. Rajan, A. Rockett, A. Arehart, and S. Marsillac, "Characterization of Electronic Defects in RbF treated CIGS Solar cells," in *2018 IEEE 7th World Conference on Photovoltaic Energy Conversion (WCPEC) (A Joint Conference of 45th IEEE PVSC, 28th PVSEC & 34th EU PVSEC), 10-15 June 2018*, Piscataway, NJ, USA, 2018: IEEE, in 2018 IEEE 7th World Conference on Photovoltaic Energy Conversion (WCPEC) (A Joint Conference of 45th IEEE PVSC, 28th PVSEC 34th EU PVSEC), pp. 1906-8, doi: 10.1109/PVSC.2018.8548277. [Online]. Available: http://dx.doi.org/10.1109/PVSC.2018.8548277

[13] S. Karki *et al.*, "In situ and ex situ investigations of KF postdeposition treatment effects on CIGS solar cells," *IEEE Journal of Photovoltaics,* vol. 7, no. 2, pp. 665-9, 03/ 2017, doi: 10.1109/JPHOTOV.2016.2637659.

[14] O. Ayala *et al.*, "Modeling of the effect of substrate temperature on Na diffusion through molybdenum films," in *44th IEEE Photovoltaic Specialist Conference, PVSC 2017, June 25, 2017 - June 30, 2017*, 2660 Woodley Road NW, Washington, DC, United states, 2017: Institute of Electrical and Electronics Engineers Inc., in 2017 IEEE 44th Photovoltaic Specialist Conference, PVSC 2017, pp. 1-3, doi: 10.1109/PVSC.2017.8366485. [Online]. Available: http://dx.doi.org/10.1109/PVSC.2017.8366485

[15] P. P. Martin, J. Lyding, and A. Rockett, "Scanning tunneling spectroscopy of epitaxial silver indium diselenide," (in English), *Surface Science,* vol. 636, pp. 8-12, Jun 2015, doi: 10.1016/j.susc.2015.01.012.

[16] S. Soltanmohammad, J. Wands, R. Farshchi, D. Poplavskyy, and A. Rockett, "Structure and phase composition of sputter deposited (Ag,Cu)(In,Ga)Se2 thin film solar cells," in *2018 IEEE 7th World Conference on Photovoltaic Energy Conversion (WCPEC) (A Joint Conference of 45th IEEE PVSC, 28th PVSEC & 34th EU PVSEC), 10-15 June 2018*, Piscataway, NJ, USA, 2018: IEEE, in 2018 IEEE 7th World Conference on Photovoltaic Energy Conversion (WCPEC) (A Joint Conference of 45th IEEE PVSC, 28th PVSEC 34th EU PVSEC), pp. 0852-5, doi: 10.1109/PVSC.2018.8547999. [Online]. Available: http://dx.doi.org/10.1109/PVSC.2018.8547999

[17] S. Karki *et al.*, "Impact of water ingress on molybdenum thin films and its effect on Cu(In,Ga)Se2 solar cells," *IEEE Journal of Photovoltaics,* vol. 10, no. 2, pp. 696-702, 03/ 2020, doi: 10.1109/JPHOTOV.2019.2959947.

[18] G. Rajan *et al.*, "Study of Instabilities and Degradation due to Moisture Ingress in the Molybdenum back contact of Cu(In,Ga)Se2 Solar Cells," in *2018 IEEE 7th World Conference on Photovoltaic Energy Conversion (WCPEC) (A Joint Conference of 45th IEEE PVSC, 28th PVSEC & 34th EU PVSEC), 10-15 June 2018*, Piscataway, NJ, USA, 2018: IEEE, in 2018 IEEE 7th World Conference on Photovoltaic Energy Conversion (WCPEC) (A Joint Conference of 45th IEEE PVSC, 28th PVSEC 34th EU PVSEC), pp. 3037-9, doi: 10.1109/PVSC.2018.8547368. [Online]. Available: http://dx.doi.org/10.1109/PVSC.2018.8547368

[19] P. K. Paul, S. Karki, G. Rajan, S. Marsillac, and A. R. Arehart, "Impact of moisture ingress on the degradation and trap spectrum in Cu(In,Ga)Se2 solar cells," in *2018 IEEE 7th World Conference on Photovoltaic Energy Conversion (WCPEC) (A Joint Conference of 45th IEEE PVSC, 28th PVSEC & 34th EU PVSEC), 10-15 June 2018*, Piscataway, NJ, USA, 2018: IEEE, in 2018 IEEE 7th World Conference on Photovoltaic Energy Conversion (WCPEC) (A Joint Conference of 45th IEEE PVSC, 28th PVSEC 34th EU PVSEC), pp. 2623-6, doi: 10.1109/PVSC.2018.8547326. [Online]. Available: http://dx.doi.org/10.1109/PVSC.2018.8547326

[20] G. Rajan *et al.*, "Understanding Instabilities and Degradation Due to Moisture Ingress in Cu(In, Ga)Se2 Solar Cells," in *2017 IEEE 44th Photovoltaic Specialists Conference (PVSC), 25-30 June 2017*, Piscataway, NJ, USA, 2017: IEEE, in 2017 IEEE 44th Photovoltaic Specialist Conference (PVSC), pp. 0182-5, doi: 10.1109/PVSC.2017.8366173. [Online]. Available: http://dx.doi.org/10.1109/PVSC.2017.8366173

[21] T. Ashrafee *et al.*, "Effect of Annealing on Molybdenum Films used as a Back Contact for Cu(In,Ga)Se-2 Solar Cells," (in English), *Ieee Phot Spec Conf,* pp. 1415-1417, 2016. [Online]. Available: <Go to ISI>://WOS:000399818701088.

[22] T. Ashrafee *et al.*, "Characterization of Cd1-xZnxS buffer layers deposited by CBD for CIGS solar cell application," in *2016 IEEE 43rd Photovoltaic Specialists Conference (PVSC), 5-10 June 2016*, Piscataway, NJ, USA, 2016: IEEE, in 2016 IEEE 43rd Photovoltaic Specialists Conference (PVSC), pp. 1418-20, doi: 10.1109/PVSC.2016.7749849. [Online]. Available: http://dx.doi.org/10.1109/PVSC.2016.7749849

[23] B. Belfore, O. Ayala, T. Ashrafee, G. Rajan, S. Karki, and S. Marsillac, "Modeling Diffusion of Impurities in Molybdenum Thin Films as a Function of Substrate Temperature," *IEEE Journal of Photovoltaics,* vol. 9, no. 1, pp. 339-43, 01/ 2019, doi: 10.1109/JPHOTOV.2018.2882211.

[24] D. J. Schroeder, J. L. Hernandez, G. D. Berry, and A. A. Rockett, "Hole transport and doping states in epitaxial Culn(1-x)Ga(x)Se(2)," (in English), *Journal of Applied Physics,* vol. 83, no. 3, pp. 1519-1526, Feb 1 1998, doi: Doi 10.1063/1.366860.

[25] D. Schroeder and A. Rockett, "Electronic effects of sodium in epitaxial CuIn1-xGaxSe2," *Journal of Applied Physics,* vol. 82, no. 10, pp. 4982-4985, NOV 15 1997 1997, doi: 10.1063/1.366365.

[26] D. Liao and A. Rockett, "Epitaxial growth of Cu(In,Ga)Se-2 on GaAs(110)," (in English), *Journal of Applied Physics,* vol. 91, no. 4, pp. 1978-1983, Feb 15 2002, doi: Doi 10.1063/1.1434549.

[27] M. Bar, S. Nishiwaki, L. Weinhardt, S. Pookpanratana, W. N. Shafarman, and C. Heske, "Electronic level alignment at the deeply buried absorber/Mo interface in chalcopyrite-based thin film solar cells," *Applied Physics Letters,* vol. 93, no. 4, 2008. [Online]. Available: http://dx.doi.org/10.1063/1.2955532.

[28] D. Liao and A. Rockett, "The structure and morphology of (112)-oriented Cu(In,Ga)Se2 epitaxial films," *Journal of Applied Physics,* regular vol. 104, no. in press, 2008.

[29] O. Ayala *et al.*, "Modeling of the Effect of Substrate Temperature on Na Diffusion Through Molybdenum Films," (in English), *Ieee Phot Spec Conf,* pp. 2132-2134, 2016. [Online]. Available: <Go to ISI>://WOS:000399818702036.

[30] S. Karki *et al.*, "Investigation of traps density and position in alkali treated Cu(In,Ga)Se2 thin films and solar cells," in *2017 IEEE 44th Photovoltaic Specialists Conference (PVSC), 25-30 June 2017*, Piscataway, NJ, USA, 2017: IEEE, in 2017 IEEE 44th Photovoltaic Specialist Conference (PVSC), pp. 2446-8, doi: 10.1109/PVSC.2017.8366286. [Online]. Available: http://dx.doi.org/10.1109/PVSC.2017.8366286

[31] S. Karki *et al.*, "In-situ and ex-situ characterizations of CIGS solar cells with KF post deposition treatment," in *2017 IEEE 44th Photovoltaic Specialists Conference (PVSC), 25-30 June 2017*, Piscataway, NJ, USA, 2017: IEEE, in 2017 IEEE 44th Photovoltaic Specialist Conference (PVSC), p. 6 pp., doi: 10.1109/PVSC.2017.8366044. [Online]. Available: http://dx.doi.org/10.1109/PVSC.2017.8366044

[32] J. Wands, S. Soltanmohammad, W. Shafarman, and A. Rockett, "Investigation of the electrical properties of grain boundaries in (AgxCu1-x)(InyGa1-y)Se2," in *2019 IEEE 46th Photovoltaic Specialists Conference (PVSC), 16-21 June 2019*, Piscataway, NJ, USA, 2019: IEEE, in 2019 IEEE 46th Photovoltaic Specialists Conference (PVSC), pp. 0962-4, doi: 10.1109/PVSC40753.2019.8981173. [Online]. Available: http://dx.doi.org/10.1109/PVSC40753.2019.8981173